

Closed-loop machine learning for discovery of novel superconductors

Elizabeth A. Pogue^{a,1,2}, Alexander New^{a,1}, Kyle McElroy^a, Nam Q. Le^a, Michael J. Pekala^a, Ian McCue^e, Eddie Gienger^a, Janna Domenico^a, Elizabeth Hedrick^b, Tyrel M. McQueen^{b,c,d,2}, Brandon Wilfong^{c,d}, Christine D. Piatko^a, Christopher R. Ratto^a, Andrew Lennon^a, Christine Chung^a, Timothy Montalbano^a, Gregory Bassen^{c,d}, and Christopher D. Stiles^{a,2}

^aResearch and Exploratory Development Department, Johns Hopkins University Applied Physics Laboratory, 11100 Johns Hopkins Road, Laurel, 20723, Maryland, United States of America; ^bDepartment of Materials Science and Engineering, Johns Hopkins University, 3400 N. Charles Street, Baltimore, 21218, Maryland, United States of America; ^cDepartment of Chemistry, Johns Hopkins University, 3400 N. Charles Street, Baltimore, 21218, Maryland, United States of America; ^dInstitute for Quantum Matter, William H. Miller III Department of Physics and Astronomy, Johns Hopkins University, 3400 N. Charles Street, Baltimore, 21218, Maryland, United States of America; ^eDepartment of Materials Science and Engineering, Northwestern University, 2220 Campus Drive, Evanston, 60208, Illinois, United States of America

This manuscript was compiled on December 21, 2022

The discovery of novel materials drives industrial innovation (1), although the pace of discovery tends to be slow due to the infrequency of “Eureka!” moments (2). These moments are typically tangential to the original target of the experimental work: “accidental discoveries”. Here we demonstrate the acceleration of intentional materials discovery – targeting material properties of interest while generalizing the search to a large materials space with machine learning (ML) methods. We demonstrate a closed-loop ML discovery process targeting novel superconducting materials, which have industrial applications ranging from quantum computing to sensors to power delivery (3–6). By closing the loop, i.e. by experimentally testing the results of the ML-generated superconductivity predictions and feeding data back into the ML model to refine, we demonstrate that success rates for superconductor discovery can be more than doubled (7). In four closed-loop cycles, we discovered a new superconductor in the Zr-In-Ni system, re-discovered five superconductors unknown in the training datasets, and identified two additional phase diagrams of interest for new superconducting materials. Our work demonstrates the critical role experimental feedback provides in ML-driven discovery, and provides definite evidence that such technologies can accelerate discovery even in the absence of knowledge of the underlying physics.

Closed-loop machine learning | Superconductivity | Materials discovery

The discovery of new materials with quantum properties, like superconductivity, drives industrial and scientific advancement (8). However, the difficulty in creating novel superconductors from potential compositions has made the discovery process stochastic and unpredictable (9). For the past quarter century, statistical approaches have aimed to better understand and predict superconductivity (10), with Machine learning (ML) emerging as the preferred approach (11–15). Although ML has shown some success in predicting novel superconductors that do not exist in known databases (13–15), many remain untested because it is not clear that many of these predictions are promising (11, 12). ML models also commonly make predictions that clearly will not superconduct for reasons discussed in this paper. Previous studies have had limited success because they fail to consider the end-to-end materials discovery lifecycle. They treat materials and databases of material properties as fixed snapshots rather than evolving systems. Additionally, they neither incorporate physics nor account for the biases of experimental sciences in the training of ML models. Once a new superconductor has been identified, experimentalists generally search for superconductivity

in related materials, accelerating the discovery of new superconductors but biasing the datasets used for machine learning to favor certain families of compounds.

Here we report on combining ML techniques with materials science and physics expertise to “close the loop” of materials discovery (Figure 1). We demonstrate that previous ML models fail to generalize across diverse materials spaces (see SI), making them unlikely to identify superconductors that are dissimilar to known ones. Consequently, we alternate between ML property prediction and experimental verification to continuously improve the fidelity of ML property prediction in regimes sparsely represented by existing materials databases. Crucially, this adds both negative data (materials incorrectly predicted to be superconductors) and positive data (materials correctly predicted) to ML training, enabling the ML model’s overall representation of the space of materials to be iteratively refined. This also avoids assuming that some materials are non-superconductors without verification (13). “Closing the loop”—leveraging inputs from materials experts and experimental verification of predictions—allowed us to demonstrate the first ML-guided discovery of a novel superconductor.

Our process uses active learning (16) to iteratively select data points to be added to a training set, with the overall goal of identifying materials with desirable properties. After ML model prediction, we use human domain expertise to further filter predicted candidates to those deemed most likely to superconduct. We engaged in a small number of total prediction/experimental measurement iterations; to maximize the superconducting transition temperatures (T_c s) of superconductors discovered over further iterations, we can use acquisition functions developed for Bayesian Optimization (17, 18). Our approach retains a human-in-the-loop for synthesizing and characterizing materials, but further automation is possible, involving, e.g., ML systems selecting experiments to be con-

C.S., I.M., C.P., E.G., K.M., and T.M.M. contributed to the conception of the work. E.P., B.W., T.M.M., E.G., and I.M. contributed to the setup and design of experiments. E.P., E.H., I.M., and B.W. synthesized samples. A.N. created the ML model with some contributions from M.P., C.P., and C.R. J.D., N.Q.L., C.C., and C.P. contributed to preparation of the datasets and integrating them with the workflow. E.P., A.N., C.S., K.M. and T.M.M. heavily contributed to the writing and revising of the manuscript. E.H., E.P., E.G., C.C., T.M.M. and B.W. collected and analyzed experimental data. E.P., C.P., A.N., T.M.M., and G.B. introduced new ways of visualizing the data. C.S., C.R., and A.L. provided guidance on research direction and communication of results. C.R. advised the team on appropriate ML techniques for property prediction and A.L. advised the team on material structure-property relationships. C.S. was involved in all aspects of this project, providing overall leadership and helping to troubleshoot technical challenges.

The authors declare no competing interests.

¹E.A.P. contributed equally to this work with A.N.

²To whom correspondence should be addressed. E-mail: Lisa.Pogue@jhuapl.edu ; mcqueen@jhu.edu ; Christopher.Stiles@jhuapl.edu

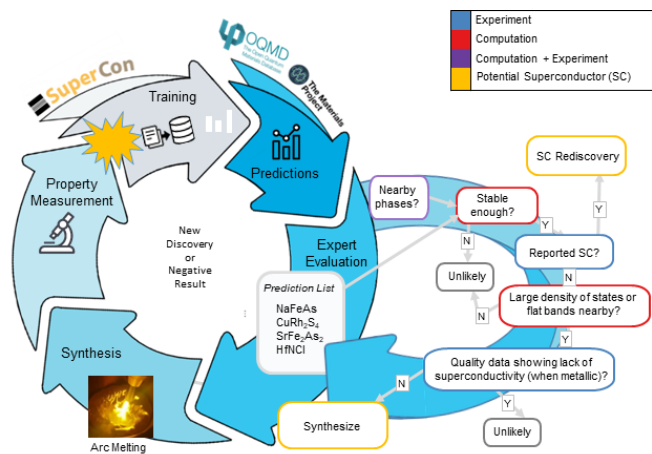


Fig. 1. ML Prediction-expert evaluation-experimental measurement loop and expert evaluation process. We closed the ML prediction-experimental measurement loop four times in this study. To improve success, experts evaluated lists of predicted superconductors following the procedure outlined to the right to determine which predictions were most promising. When evaluating these predictions, the data sources referenced are denoted by color. “Experiment” includes both literature data and prior but unpublished internal data. “Computation” includes data from computational databases, computed literature data, and targeted computational data that we acquired.

ducted, or robot-powered self-driving laboratories (19–21).

We confirmed our approach by rediscovering five superconductors outside of the ML model’s training set. Through closing the prediction-experimental measurement loop four times, we discovered a new superconductor in the Zr-In-Ni phase diagram, and identified two other phase diagrams of interest (Zr-In-Cu and Zr-Fe-Sn). These materials come from a wide variety of families: iron pnictides, doped 2D ternary transition metal nitride halides, intermetallics, and spinels.

1. ML Models for predicting superconductivity

For the initial prediction step of the closed-loop approach, we trained an ML model to predict the superconducting transition temperature, T_c , of candidate materials. Our primary source of training data, SuperCon (22), contains compositions of known superconductors. Only the materials’ compositions were used to train the ML model for predicting T_c since SuperCon did not contain additional usable information. Materials Project (MP) (23) and Open Quantum Materials Database (OQMD) (24), some of the largest public sets of computational materials data, supplied candidate compositions to be screened for superconductivity. These two databases do not contain any T_c data. These three datasets are visualized in Figure 2 using a joint representation. Crucially, the amount of data for which we have superconducting information is much smaller than our other sources of data and is not uniformly sampled across the joint space.

It is well-known (27) that when ML methods make predictions on data outside of their training data distribution, accuracy often suffers; this is often called the *out-of-distribution generalization problem*. In cheminformatics (28), it is common to assess whether a dataset is within the distribution of a training dataset by seeing how far, in some representative metric space, its points are from the training dataset: as the difference between the distribution of new data and the training data increases, the likelihood that a model will accurately

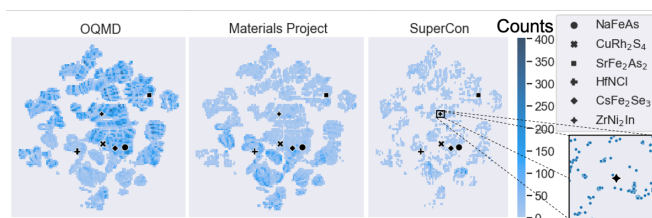


Fig. 2. Visualization of OQMD, Materials Project and SuperCon Databases together. A histogram of the concentration of materials from a Uniform Manifold and Projection (UMAP) (25) embedding of OQMD (without superconductivity information), MP (without superconductivity information), and SuperCon (superconductivity information), based on Magpie (26) descriptors for the datasets. The embedding is learned from concatenation of Magpie descriptors obtained from all three datasets; the same axis limits are used across each subplot. T_c is not part of the Magpie descriptors and, therefore, did not influence the representation. The six black symbols indicate five rediscovered superconductors (Section 4), and our novel superconductor, near ZrNi₂In. The inset on the right highlights the local region in which ZrNi₂In is found, which is sparse and far from the rediscovered superconductors.

predict their properties decreases. To improve assessment of generalization, out-of-distribution data may be simulated by creating validation sets that split based on non-random criteria like Murcko scaffold (29) or cluster identity, the latter being the leave-one-cluster-out cross-validation (LOCO-CV) strategy (30). In the Supplementary Information and Extended Data, we apply LOCO-CV in a simulated superconductor-identification problem. We show that a strong ML model fails to make accurate predictions of superconducting status on out-of-distribution data. This motivates our need for multiple iterations of model training, candidate selection, candidate synthesis, and model retraining.

We rely on a recent ML model for chemical property prediction, Representation learning from Stoichiometry (RooSt) (see Methods and SI), to predict a material’s superconductivity using only its stoichiometry (i.e., ignoring the material’s crystal structure). This was necessary because the SuperCon database used for training contains insufficient structural information for more expressive ML models, such as the crystal graph convolutional neural network (31, 32). The intersection of SuperCon with MP and OQMD was not large enough to allow us to easily estimate the corresponding structure.

A. Identifying new predicted superconductors using ML. Following the training of an ensemble of RooSt models using the SuperCon database, we apply them to our set of potential superconductors (i.e., MP and OQMD). We filter for materials likely to be high- T_c superconductors (see Methods, Extended Data, and SI).

A risk of searching for new superconductors from a static list of candidates is that while a material in MP or OQMD may not have the exact composition as a superconductor, it may have a composition extremely close in terms of stoichiometry, such as MgB₂ vs. Mg₃₃B₆₇. Thus, every time we produce a new list of candidates, we identify each candidate’s minimal Euclidean distance, in Magpie-space (26), to any point in our training data, and we remove candidates too close to SuperCon. This distance is used by domain experts as one of the metrics to select final candidates to synthesize and test.

2. Incorporating domain expertise

It is not practical to experimentally verify all ML predictions. The costs associated with fabricating and characterizing a new material are high; hence we are only able to experimentally analyze a small subset of the ML predictions. Expert analysis to factor in information not present in the ML training data (Figure 1) was key for achieving high success rates.

The Materials Project and OQMD databases both contain calculated stability information not used by the ML model. Of 190 predicted superconductors in a given prediction round, only 39 compounds were calculated to be stable ($E_{\text{over hull}} = 0.00 \text{ eV/atom}$) but 83 were nearly stable ($E_{\text{over hull}} < 0.05 \text{ eV/atom}$). Stable materials and those with prior experimental reports were prioritized to increase the likelihood that targeted compounds could be successfully synthesized. Prioritizing these materials ensured that failures to observe superconductivity were indicative of the behavior of the targeted compound rather than a failure to synthesize that compound.

Insulating materials like $\beta\text{-ZrNCI}$ and the cuprates superconductor with high T_c s because they can be doped into a metallic state (33). One long-running challenge for machine-learning approaches to predicting high- T_c superconductivity is that large bandgap insulators incapable of superconductivity tend to be given overweighted classification scores, likely due to the high T_c s of the cuprates(15). Therefore, metals and easily doped materials were favored for testing. Similarly, for some predicted metals, we investigated nearby compounds with similar structures that were known in literature but were not found in Materials Project or OQMD (e.g.: $\text{Zr}_3\text{Fe}_4\text{Sn}_4$ and $\text{Hf}_3\text{Fe}_4\text{Sn}_4$ (34, 35)) and isostructural compounds with promising band structures (e.g.: ZrNi_2In).

Since the T_c s of compounds are very sensitive to alloy disorder and lattice parameter, we explored several compositions near each prediction (36). We also considered the ease and safety of synthesizing the target materials (e.g., by excluding extremely high-pressure syntheses). Powder X-ray diffraction (XRD) was used to ensure that the target material was successfully made and temperature-dependent AC magnetic susceptibility was used to screen for superconductivity. Superconductors are perfectly diamagnetic below their T_c with no (or minimal) applied field.

3. High-throughput experimental evaluation of T_c using A15 phases

To illustrate the sensitivity of experimentally-measured T_c s to processing conditions, we made and tested samples with A_3B stoichiometry (Figure 3a), including many known superconductors from the A15 family (44). Similar compositional sensitivity is common in other systems beyond A15 compounds. For example, as x varies between 0 and 0.35, $\text{La}_{2-x}\text{Sr}_x\text{CuO}_4$ can vary from not superconducting to having a T_c up to 36 K (14). Our experiments show that high-throughput synthesis and characterization techniques can reliably and quickly screen systems for superconductivity. Optimization of many superconducting phases requires much lower-throughput techniques for phase-pure and fully-superconducting samples.

4. Rediscovered Superconductors

Using this closed-loop method and high-throughput synthesis, we re-discovered five known superconductors that were not represented in the ML training dataset. A list of these is found in Table 1. Many of these superconduct when doped or at elevated pressures, illustrating the challenges of capturing doping effects and ruling out superconductivity purely on the basis of a negative result at atmospheric pressure.

We have experimentally sampled less than 100 different compounds and have been able to re-discover five previously reported (outside of the ML training set) superconductors and are investigating one novel superconductor and two new potential superconductors, demonstrating a much higher success rate than current exclusively human-lead approaches. A group of several teams of experts in Hosono et al. achieved a success rate of $\sim 3\%$ with 1000+ different compounds synthesized, in the wake of their discovery of iron-based superconductors in 2006 (7). Furthermore since, unlike conventional exclusively expert-driven investigations, our inputs are not limited to a single or few classes of materials, ML identifies potential families of candidate superconductor materials that may not have otherwise been explored.

Table 1. Superconductors rediscovered by machine learning. Since the model only took stoichiometry into account, predictions where small stoichiometry changes led to superconductivity were considered successful discoveries.

Compound	Iteration	Database and Comments	T_c
NaFeAs	2	Materials Project, reduced topotactically in water	25 K (37)
CuRh_2S_4	2	Materials Project	4.7 K (38)
SrFe_2As_2	2	Materials Project, reduced topotactically in water	25 K (39)
HfNCI	3 and 4	Materials Project, OQMD, intercalated by lithium	40 K (40)
CsFe_2Se_3	3	Analogs $\text{CsFe}_{4-x}\text{Se}_4$ (5 K, $> \sim 34.55 \text{ GPa}$) (41), BaFe_2Se_3 (11 K, $> \sim 12.7 \text{ GPa}$) (42), and BaFe_2S_3 (24 K, $> \sim 10 \text{ GPa}$) (43)	

5. New superconductor in Zr-In-Ni phase diagram

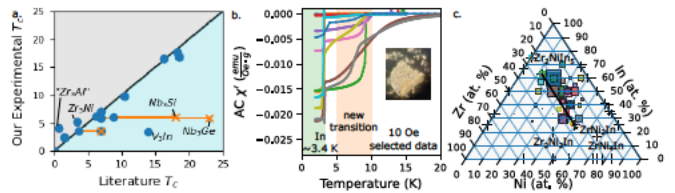


Fig. 3. Experimental visualizations of superconductivity in A15 compounds and in the Zr-In-Ni system. (a) Evaluation of our high-throughput synthesis of compounds with A_3B stoichiometry (including A15 compounds) demonstrates the effects of processing on the measured T_c and our ability to positively identify superconductors quickly. To track down the new superconductor in the Zr-In-Ni phase diagram, samples were tested from around the phase diagram (b and c) and the transition magnitude between 5 and 10 K (orange region) was used to scale data points. This transition was distinct from the indium-related transition (green). The strength of the indium signal could be used as a calibration to determine the relative strength of the higher-temperature signal. The line in (c) connects Zr_2NiIn_5 and ZrNi_2In . The compositions of samples with the strongest superconducting signals fell near this line. The colors in b, c, and Figure S5 and the symbols in b and Figure S5 match. The inset in (b) shows a piece of the sample with the strongest superconducting signal we observed.

Our novel ML-driven process discovered a new superconducting phase in the Zr-In-Ni system with a T_c of $\sim 9 \text{ K}$ (Figure 1b-c and Extended Data). No other known elements,

binaries or ternaries in the Zr-In-Ni system would explain a superconducting transition temperature this high and the elements and binaries have been extensively investigated (11, 44–46).

We synthesized many of these binaries and did not see evidence of superconductivity above 2 K unrelated to indium. A small, very broad diamagnetic signal was observed in a ZrIn_3 sample that went away upon annealing. The intensity of the superconducting signal was largest for indium and nickel-rich compositions connecting ZrNi_2In and Zr_2NiIn_5 stoichiometries. The phases present in these arc melted samples matched well upon Rietveld refinement with ZrNi_2In , $\text{Zr}_2\text{Ni}_2\text{In}$, and In (See Extended Data, $R_{wp}=1.25\%$).

Magnetic susceptibility measurements for ZrNi_2In reported in 1999 showed no evidence of a superconducting signal (47). However, in 2004, members of the same group presented at E-MRS that ZrNi_2In superconducts with a T_c of 9 K (48), suggesting there is variability in the system (There is no archival paper that we could locate and no data is readily available.) The isostructural compounds ZrNi_2Ga and ZrNi_2Al superconduct with a T_c of 2.9 K and 1.38 K, respectively (49, 50). Their superconductivity has been attributed to a Van Hove singularity at the L point near the Fermi level that should also be present in ZrNi_2In (23, 49). The atom contributing to these states is primarily nickel; moving down the periodic table to indium from gallium should not change these states significantly. Nearly phase-pure ZrNi_2In had a weak signal compared to more In-rich compositions, indicating that the superconducting phase observed here is not due to stoichiometric ZrNi_2In .

The phase spaces near ZrNi_2In and ZrCu_2In would not have been identified as a place to look for higher-temperature superconductors, because Heusler alloys tend to have T_c 's well below 5 K. Our experimental investigation also revealed that the Zr-Cu-In and Zr-Fe-Sn systems merit further investigation (see Extended Data and SI).

6. Conclusions

We have presented the first ever closed-loop ML-based directed discovery of a novel superconductor with experimental verification (within the Zr-Ni-In system), identified two additional systems of interest (Zr-Cu-In and Zr-Fe-Sn), and rediscovered five others not represented in our ML training set.

Past revolutionary discoveries tended to happen by serendipity, finding something in material families outside of what was known at the time. Our approach, relying only on stoichiometry and a measure of “distance” from what is currently known, is more likely to find novel materials of interest and a sense of where unexplored but promising materials lie compared to ML-guided approaches that proceed within only a given family of materials.

This approach improves performance with experience, in that with every closing of the loop, the ML model undergoes feedback and refinement, enabling efficient exploration of materials space. These improvements ultimately will reduce the cost of materials development and discovery. The success of this approach has been demonstrated by discoveries and rediscoveries coming from vastly different families, illustrating the potential of this tool for the discovery of novel materials with targeted properties. This methodology can be expanded to target more than one desired property, and applied to domains

beyond superconductors as long as a mechanism for new data acquisition based on ML-based predictions can be leveraged.

Materials and Methods

A. Data. Our general data source containing the superconducting transition temperature, T_c of many known compounds is the SuperCon database (22), published by the Japanese National Institute for Materials Science. More details are available in the SI.

In this work, we use the version of SuperCon released by Stanev *et al.* (11), available online. This contains 16,414 material compositions and associated critical temperature measurements. However, some of these compositions are invalid (e.g., $\text{Y}_2\text{C}_2\text{Br}_{0.5}\text{I}_{1.5}$) and were removed prior to analysis. Our final training dataset has 16,304 valid compositions. In the Extended Data and the SI, we give additional detail about our training dataset. Figure S1 shows the distribution of T_c values in our training data—note that the distribution is weighted toward low- T_c compositions.

We use MP (23) and OQMD(24) as the set of candidates to screen with ML for superconducting potential. MP and OQMD are some of the largest public sets of computational materials data. Their records contain full crystallographic information for material structures, along with some associated electronic and mechanical properties (but not, importantly, T_c). We scraped MP for material records present in it as of October 2020 using the `MPester` class from the `pymatgen` (51) package. We later downloaded the entire OQMD v1.4 database. The Extended Data contains a table of MP and OQMD material IDs used in this study.

B. Computational Methods and Uncertainty. RooSt (52) is a graph neural network (53) that relates material composition to properties by applying a message-passing scheme (54) to a weighted graph representation of the composition’s stoichiometry, producing a real-valued embedding vector. To make a prediction, this embedding is then passed through a feedforward network.

In this work, we make use of the publicly-available implementation of RooSt, which is implemented in PyTorch (55). Furthermore, we use the default hyperparameters recommended by the RooSt authors, including basing the initial species representation vectors on the *matscholar* embedding (56). Since we seek materials likely to be high- T_c superconductors, and we expect RooSt’s classification model to poorly generalize on out of distribution data, we filter for materials predicted to be in the highest T_c tertile ($T_c \geq 20$ K) with a classification score of at least 0.66 (see SI).

RooSt models incorporate two sources of uncertainty in their T_c predictions: We account for aleatoric uncertainty (randomness of input data) by letting a model estimate a mean and standard deviation for each label’s logit (57), and we incorporate epistemic uncertainty (error in the model’s result, itself) by averaging over an ensemble of independently trained RooSt models (58).

C. Experiment. To synthesize compounds in a medium-throughput manner, arc melting and solid state techniques were used. The standard sample size was 500-700 mg. A list of precursors used in this project is found in Table S3 in the SI and details of the synthetic procedures are found in the SI. Additional heat treatments were performed on an as-needed basis when isolating superconducting phases.

Powder X-ray diffraction patterns were collected at room temperature on the as-melted samples using a Bruker D8 Focus powder diffractometer with $\text{Cu-K}\alpha$ radiation ($\lambda_{k,\alpha,1} = 1.540596 \text{ \AA}$, $\lambda_{k,\alpha,2} = 1.544493 \text{ \AA}$), Soller slits, and a LynxEye detector to verify the presence of the target phase. We measured from $2\theta=5^\circ-60^\circ$ with a step size of 0.018563° over 4 minutes as an initial screen. When gathering XRD patterns of samples in preparation for Rietveld refinement, 4 h measurements were performed from $2\theta=5^\circ-120^\circ$ with a step size of 0.01715° .

AC-susceptibility measurements were conducted using either a Quantum Design Magnetic Properties Measurement (MPMS) System ($H_{DC} = 10$ Oe, $H_{AC} = 1-3$ Oe, 900 Hz) or a Quantum Design Physical Properties Measurement (PPMS) System ($H_{DC} = 10$ Oe,

$H_{AC}=3$ Oe, 1 kHz), measuring $T \geq 2$ K. Since prior density function theory (DFT) calculations (59) suggested that CaAg_2Ge_2 would superconduct near $T = 1.5$ K, we used the ^3He option with the MPMS to measure from 0.4 K to 1.7 K for that sample in addition to our standard measurement above 2 K.

ACKNOWLEDGMENTS. The authors gratefully acknowledge internal financial support from the Johns Hopkins University Applied Physics Laboratory's Independent Research & Development (IR&D) Program for funding portions of this work. The MPMS3 system used for magnetic characterization was funded by the National Science Foundation, Division of Materials Research, Major Research Instrumentation Program, under Grant #1828490.

- National Research Council, *Frontiers in Crystalline Matter*. Washington, DC: The National Academies Press (2009). <https://doi.org/10.17226/12640>
- National Science and Technology Council, Materials Genome Initiative Strategic Plan: A Report by the Subcommittee on the Materials Genome Initiative Committee on Technology of the National Science and Technology Council. (2021). <https://www.mgi.gov/sites/default/files/documents/MGI-2021-Strategic-Plan.pdf>
- Zhao, H., Li, H., Ortiz, B.R., Teicher, S.M., Park, T., Ye, M., Wang, Z., Balents, L., Wilson, S.D., Zeljkovic, I., Cascade of correlated electron states in the kagome superconductor CsV_3Sb_5 . *Nature* **599**, 216–221 (2021). <https://doi.org/10.1038/s41586-021-03946-w>
- Li, Y., Xu, X., Lee, M.-H., Chu, M.-W., Chien, C.L., Observation of half-quantum flux in the unconventional superconductor beta- Bi_2Pd . *Science* **366**(6462), 238–241 (2019). <https://doi.org/10.1126/science.aau6539>
- Mather, J.C., Super photon counters. *Nature* **401**, 654–655 (1999). <https://doi.org/10.1038/44301>
- Grant, P., Rehearsals for prime time. *Nature* **411**, 532–533 (2001). <https://doi.org/10.1038/35079212>
- Hosono, H., Tanabe, K., Takayama-Muromachi, E., Kageyama, H., Yamanaka, S., Kumakura, H., Nohara, M., Hiramatsu, H., Fujitsu, S.: Exploration of new superconductors and functional materials, and fabrication of superconducting tapes and wires of iron pnictides. *Science and Technology of Advanced Materials* **16**(3) (2015). <https://doi.org/10.1088/1468-6996/16/3/033503>
- de Pablo, J.J., Jackson, N.E., Webb, M.A., Chen, L.-Q., Moore, J.E., Morgan, D., Jacobs, R., Pollock, T., Schlom, D.G., Toberer, E.S., Analysis, J., Dabo, I., DeLongchamp, D.M., Fiete, G.A., Grason, G.M., Hautier, G., Mo, Y., Rajan, K., Reed, E.J., Rodriguez, E., Stevanovic, V., Suntivich, J., Thornton, K., Zhao, J.-C.: New frontiers for the materials genome initiative. *npj Computational Materials* **5**(1), 41 (2019). <https://doi.org/10.1038/s41524-019-0173-4>
- Mandrus, D.: Gifts from the superconducting curiosity shop. *Frontiers of Physics* **6**(4), 347–349 (2011). <https://doi.org/10.1007/s11467-011-0226-8>
- Hirsch, J.: Correlations between normal-state properties and superconductivity. *Physical Review B - Condensed Matter and Materials Physics* **55**(14), 9007–9024 (1997). <https://doi.org/10.1103/PhysRevB.55.9007>
- Stanev, V., Oses, C., Kusne, A.G., Rodriguez, E., Paglione, J., Curtarolo, S., Takeuchi, I.: Machine learning modeling of superconducting critical temperature. *npj Computational Materials* **2018** 4:1 4, 1–14 (2018). <https://doi.org/10.1038/s41524-018-0085-8>
- Zeng, S., Zhao, Y., Li, G., Wang, R., Wang, X., Ni, J.: Atom table convolutional neural networks for an accurate prediction of compounds properties. *npj Comput Mater* **5**(1), 84 (2019). <https://doi.org/10.1038/s41524-019-0223-y>. Accessed 2021-10-28
- Konno, T., Kurokawa, H., Nabeshima, F., Sakishita, Y., Ogawa, R., Hosako, I., Maeda, A.: Deep Learning Model for Finding New Superconductors. *Phys. Rev. B* **103**(1), 014509 (2021). <https://doi.org/10.1103/PhysRevB.103.014509>. arXiv: 1812.01995. Accessed 2021-10-11
- Roter, B., Dordovic, S.V.: Predicting new superconductors and their critical temperatures using machine learning. *Physica C: Superconductivity and its Applications* **575**, 1353689 (2020). <https://doi.org/10.1016/j.physc.2020.1353689>. Accessed 2021-10-11
- Quinn, M.R., McQueen, T.M.: Identifying New Classes of High Temperature Superconductors With Convolutional Neural Networks. *Frontiers in Electronic Materials* **2**(May), 1–12 (2022). <https://doi.org/10.3389/femat.2022.893797>
- Lookman, T., Balachandran, P.V., Xue, D., Yuan, R.: Active learning in materials science with emphasis on adaptive sampling using uncertainties for targeted design. *npj Computational Materials* **5**(1), 21 (2019). <https://doi.org/10.1038/s41524-019-0153-8>
- Attia, P.M., Grover, A., Jin, N., Severson, K.A., Markov, T.M., Liao, Y.-H., Chen, M.H., Cheong, B., Perkins, N., Yang, Z., Herring, P.K., Aykol, M., Harris, S.J., Braatz, R.D., Ermon, S., Chueh, W.C.: Closed-loop optimization of fast-charging protocols for batteries with machine learning. *Nature* **578**(7795), 397–402 (2020). <https://doi.org/10.1038/s41586-020-1994-5>
- Zhang, Y., Apley, D.W., Chen, W.: Bayesian optimization for materials design with mixed quantitative and qualitative variables. *Scientific Reports* **10**(1), 4924 (2020). <https://doi.org/10.1038/s41598-020-60652-9>
- Coley, C.W., Eyke, N.S., Jensen, K.F.: Autonomous discovery in the chemical sciences part 1: Progress. *Angewandte Chemie International Edition* **59**(51), 22858–22893 (2020) <https://onlinelibrary.wiley.com/doi/pdf/10.1002/anie.201909987>. <https://doi.org/10.1002/anie.201909987>
- Stach, E., deCost, B., Kusne, A.G., Hatrick-Simpers, J., Brown, K.A., Reyes, K.G., Schrier, J., Billinge, S., Buonassisi, T., Foster, I., Gomes, C.P., Gregoire, J.M., Mehta, A., Montoya, J., Olivetti, E., Park, C., Rotenberg, E., Saikin, S.K., Smullin, S., Stanev, V., Maruyama, B.: Autonomous experimentation systems for materials development: A community perspective. *Matter* **4**(9), 2702–2726 (2021). <https://doi.org/10.1016/j.matt.2021.06.036>
- MacLeod, B.P., Parlange, F.G.L., Morrissey, T.D., Häse, F., Roch, L.M., Dettelbach, K.E., Moreira, R., Yunker, L.P.E., Rooney, M.B., Deeth, J.R., Lai, V., Ng, G.J., Situ, H., Zhang, R.H., Elliott, M.S., Haley, T.H., Dvorak, D.J., Aspuru-Guzik, A., Hein, J.E., Berlinguette, C.P.: Self-driving laboratory for accelerated discovery of thin-film materials. *Science Advances* **6**(20), 8867 (2020) <https://www.science.org/doi/pdf/10.1126/sciadv.aaz8867>. <https://doi.org/10.1126/sciadv.aaz8867>
- SuperCon (1988). <https://supercon.nims.go.jp/> Accessed 2021
- Jain, A., Ong, S.P., Hautier, G., Chen, W., Richards, W.D., Dacek, S., Cholia, S., Gunter, D., Skinner, D., Ceder, G., Persson, K.A.: Commentary: The materials project: A materials genome approach to accelerating materials innovation. *APL Materials* **1**, 011002 (2013). <https://doi.org/10.1063/1.4812323>
- Saal, J.E., Kirklın, S., Aykol, M., Meredig, B., Wolverton, C.: Materials design and discovery with high-throughput density functional theory: The open quantum materials database (oqmd). *JOM* **65**(11), 1501–1509 (2013). <https://doi.org/10.1007/s11837-013-0755-4>
- McInnes, L., Healy, J., Melville, J.: UMAP: Uniform Manifold Approximation and Projection for Dimension Reduction (2020). <https://arxiv.org/abs/1802.03426>
- Ward, L., Agrawal, A., Choudhary, A., Wolverton, C.: A general-purpose machine learning framework for predicting properties of inorganic materials. *npj Computational Materials* **2**(1), 16028 (2016). <https://doi.org/10.1038/npjcompumats.2016.28>
- Gulrajani, I., Lopez-Paz, D.: In search of lost domain generalization. In: International Conference on Learning Representations (2021). <https://openreview.net/forum?id=QdXeXDoWtl>
- Liu, R., Wallqvist, A.: Molecular similarity-based domain applicability metric efficiently identifies out-of-domain compounds. *Journal of Chemical Information and Modeling* **59**(1), 181–189 (2019) <https://doi.org/10.1021/acs.jcim.8b00597>. <https://doi.org/10.1021/acs.jcim.8b00597>. PMID: 30404432
- Bemis, G.W., Murcko, M.A.: The properties of known drugs. 1. molecular frameworks. *Journal of Medicinal Chemistry* **39**(15), 2887–2893 (1996). <https://doi.org/10.1021/jm9602928>
- Meredig, B., Antono, E., Church, C., Hutchinson, M., Ling, J., Paradiso, S., Blaiszik, B., Foster, I., Gibbons, B., Hatrick-Simpers, J., Mehta, A., Ward, L.: Can machine learning identify the next high-temperature superconductor? examining extrapolation performance for materials discovery. *Mol. Syst. Des. Eng.* **3**, 819–825 (2018). <https://doi.org/10.1039/C8ME00012C>
- Xie, T., Grossman, J.C.: Crystal graph convolutional neural networks for an accurate and interpretable prediction of material properties. *Phys. Rev. Lett.* **120**, 145301 (2018). <https://doi.org/10.1103/PhysRevLett.120.145301>
- Park, C.W., Wolverton, C.: Developing an improved crystal graph convolutional neural network framework for accelerated materials discovery. *Phys. Rev. Materials* **4**, 063801 (2020). <https://doi.org/10.1103/PhysRevMaterials.4.063801>
- Fournier, P.: T and infinite-layer electron-doped cuprates. *Physica C: Superconductivity and its Applications* **514**, 314–338 (2015). <https://doi.org/10.1016/j.physc.2015.02.036>
- Calta, N.P., Kanatzidis, M.G.: $\text{Hg}_2\text{Fe}_2\text{Sn}_4$ and $\text{Hg}_2\text{Fe}_{4-x}\text{Sn}_{10+x}$: Two stannide intermetallics with low-dimensional iron sublattices. *Journal of Solid State Chemistry* **236**, 130–137 (2016). <https://doi.org/10.1016/j.jssc.2015.12.017>
- Savidan, J.C., Joubert, J.M., Tofflon-Masclat, C.: An experimental study of the Fe-Sn-Zr ternary system at 900°C. *Intermetallics* **18**(11), 2224–2228 (2010). <https://doi.org/10.1016/j.intermet.2010.07.007>
- Matthias, B.T., Geballe, T.H., Willens, R.H., Corenzwitt, E., Hull, J. G.W.: Superconductivity in Nb_3Ge . *Physical Review* **139**(5A), 1501–1503 (1965)
- Todorov, I., Chung, D.Y., Claus, H., Malliakas, C.D., Douvalis, A.P., Bakas, T., He, J., Dravid, V.P., Kanatzidis, M.G.: Topotactic redox chemistry of NaFeAs in water and air and superconducting behavior with stoichiometry change. *Chemistry of Materials* **22**(13), 3916–3925 (2010). <https://doi.org/10.1021/cm100252r>
- Hagino, T., Seki, Y., Wada, N., Tsuji, S., Shirane, T., Kumagai, K.I., Nagata, S.: Superconductivity in spinel-type compounds CuRh_2S_4 and CuRh_2Se_4 . *Physical Review B* **51**(18), 12673–12684 (1995). <https://doi.org/10.1103/PhysRevB.51.12673>
- Hiramatsu, H., Katase, T., Kamiya, T., Hirano, M., Hosono, H.: Water-induced superconductivity in SrFe_2As_2 . *Physical Review B - Condensed Matter and Materials Physics* **80**(5), 2–5 (2009). <https://doi.org/10.1103/PhysRevB.80.052501>
- Pamuk, B., Mauri, F., Calandra, M.: High- T_c superconductivity in weakly electron-doped HfNiCl. *Physical Review B* **96**(2), 1–7 (2017) [arXiv:1706.00854](https://arxiv.org/abs/1706.00854). <https://doi.org/10.1103/PhysRevB.96.024518>
- Si, J., Chen, G.Y., Li, Q., Zhu, X., Yang, H., Wen, H.H.: Unconventional Superconductivity Induced by Suppressing an Iron-Selenium-Based Mott Insulator CsFe_4Se_4 . *Physical Review X* **10**(4), 41008 (2020) [arXiv:2008.12191](https://arxiv.org/abs/2008.12191). <https://doi.org/10.1103/PhysRevX.10.041008>
- Ying, J., Lei, H., Petrovic, C., Xiao, Y., Struzhkin, V.V.: Interplay of magnetism and superconductivity in the compressed Fe-ladder compound BaFe_2Se_3 . *Physical Review B* **95**(24), 1–5 (2017). <https://doi.org/10.1103/PhysRevB.95.241109>
- Yamauchi, T., Hirata, Y., Ueda, Y., Ohgushi, K.: Pressure-Induced Mott Transition Followed by a 24-K Superconducting Phase in BaFe_2S_3 . *Physical Review Letters* **115**(24), 1–5 (2015). <https://doi.org/10.1103/PhysRevLett.115.246402>
- Matthias, B.T., Geballe, T.H., Compton, V.B.: Superconductivity. *Superconductivity* **35**(1), 1–22 (1963). <https://doi.org/10.1016/B978-0-12-088761-3.X5021-2>
- Shaw, R.W., Mapother, D.E., Hopkins, D.C.: Critical fields of superconducting tin, indium, and tantalum. *Physical Review* **120**(1), 88–91 (1960)
- Berger, L.I., Roberts, B.W.: Properties of Superconductors. In: Rumble, J.R. (ed.) *CRC Handbook of Chemistry and Physics*, 102nd edn., pp. 56–71. CRC Press (Taylor and Francis), Boca Raton, FL (2021). Chap. 12
- Zaremba, V., Kaczorowski, D., Gulaj, L.D.: Crystal structure, magnetic and electrical properties of ZrNi_2In and ZrCu_2In . *Journal of Alloys and Compounds* **292**, 1–3 (1999)
- Zaleski, A.J., Kaczorowski, D., Zaremba, V.I.: ZrNi_2In - New Superconducting Heusler Alloy. In: E-MRS Fall Meeting, Symposium E Poster, pp. 152–152. E-MRS, Warsaw, Poland (2004). <http://science24.com/paper/2054>
- Winterlik, J., Fecher, G.H., Felser, C., Jourdan, M., Grube, K., Hardy, F., Von Löhnysen, H., Holman, K.L., Cava, R.J.: Ni-based superconductor: Heusler compound ZrNi_2Ge . *Physical Review B - Condensed Matter and Materials Physics* **78**(18), 1–9 (2008). <https://doi.org/10.1103/PhysRevB.78.184506>
- Wernick, J.H., Hull, G.W., Geballe, T.H., Bernardini, J.E., Waszczak, J.V.: Superconductivity in ternary Heusler intermetallic compounds. *Materials Letters* **2**(2), 90–92 (1983). [https://doi.org/10.1016/0167-5768\(83\)90001-1](https://doi.org/10.1016/0167-5768(83)90001-1)

org/10.1016/0167-577X(83)90043-5

51. Ong, S.P., Richards, W.D., Jain, A., Hautier, G., Kocher, M., Cholia, S., Gunter, D., Chevrier, V.L., Persson, K.A., Ceder, G.: Python materials genomics (pymatgen): A robust, open-source python library for materials analysis. *Computational Materials Science* **68**, 314–319 (2013). <https://doi.org/10.1016/j.commatsci.2012.10.028>
52. Goodall, R.E.A., Lee, A.A.: Predicting materials properties without crystal structure: deep representation learning from stoichiometry. *Nature Communications* 2020 11:1 **11**, 1–9 (2020). <https://doi.org/10.1038/s41467-020-19964-7>
53. Wu, Z., Pan, S., Chen, F., Long, G., Zhang, C., Yu, P.S.: A comprehensive survey on graph neural networks. *IEEE Transactions on Neural Networks and Learning Systems* **32**(1), 4–24 (2021). <https://doi.org/10.1109/tnnls.2020.2978386>
54. Gilmer, J., Schoenholz, S.S., Riley, P.F., Vinyals, O., Dahl, G.E.: Neural message passing for quantum chemistry. In: *Proceedings of the 34th International Conference on Machine Learning - Volume 70. ICML'17*, pp. 1263–1272. JMLR.org, Sydney, Australia (2017). <https://doi.org/10.5555/3305381.3305512>
55. Paszke, A., Gross, S., Massa, F., Lerer, A., Bradbury, J., Chanan, G., Killeen, T., Lin, Z., Gimelshein, N., Antiga, L., Desmaison, A., Köpf, A., Yang, E.Z., DeVito, Z., Raison, M., Tejani, A., Chilamkurthy, S., Steiner, B., Fang, L., Bai, J., Chintala, S.: Pytorch: An imperative style, high-performance deep learning library. In: Wallach, H.M., Larochelle, H., Beygelzimer, A., d'Alché-Buc, F., Fox, E.B., Garnett, R. (eds.) *Advances in Neural Information Processing Systems 32: Annual Conference on Neural Information Processing Systems 2019, NeurIPS 2019, December 8-14, 2019, Vancouver, BC, Canada*, pp. 8024–8035 (2019). <https://proceedings.neurips.cc/paper/2019/file/bdbca288fee7f92f2bfa9f7012727740-Paper.pdf>
56. Tshitoyan, V., Dagdelen, J., Weston, L., Dunn, A., Rong, Z., Kononova, O., Persson, K.A., Ceder, G., Jain, A.: Unsupervised word embeddings capture latent knowledge from materials science literature. *Nature* **571**(7763), 95–98 (2019). <https://doi.org/10.1038/s41586-019-1335-8>
57. Nix, D.A., Weigend, A.S.: Estimating the mean and variance of the target probability distribution. In: *Proceedings of 1994 IEEE International Conference on Neural Networks (ICNN'94)*, vol. 1, pp. 55–601 (1994). <https://doi.org/10.1109/ICNN.1994.374138>
58. Lakshminarayanan, B., Pritzel, A., Blundell, C.: Simple and scalable predictive uncertainty estimation using deep ensembles. In: *Proceedings of the 31st International Conference on Neural Information Processing Systems. NIPS'17*, pp. 6405–6416. Curran Associates Inc., Red Hook, NY, USA (2017)
59. Sinaga, G.S., Utimula, K., Nakano, K., Hongo, K., Maezono, R.: First Principles Calculations of Superconducting Critical Temperature of ThCr₂Si₂-Type Structure. *arXiv* (2019). <https://doi.org/10.48550/ARXIV.1911.10716>

DRAFT

Supporting Information Text

A. Material descriptors. Superconducting properties of materials depend in a complex manner on their composition and structure. In this work, we make a simplifying assumption that the superconducting critical temperature of a material, T_c , can be estimated primarily based on its composition alone. Microstructure affects T_c but can be treated as a second-order effect, and is thus beyond the present scope. This assumption is commonly-made in other ML-based superconductor work (e.g., (1–3)). On the other hand, crystal structure is essential to determining superconducting properties and is not trivially derived from composition. In principle, however, stable crystal structures can be implicitly associated with each composition given thermodynamic conditions. In attempting to map composition directly to T_c , we therefore test a hypothesis that models can be trained to make those implicit associations with crystal structure as needed, given only information about composition and properties. This continues in the direction of prior work using both vector-based (2, 4, 5) and graph-based (6) representations of materials based only on composition to predict properties.

A critical challenge is therefore to implement material representations and model architectures that balance expressiveness and efficiency. That is, they should capture sufficiently complex physical information to learn subtle effects of composition on T_c , but they should not be so complex to require larger amounts of training data than practically obtainable.

B. Problem Setup and Model Validation. We formulate our prediction problem as an uncertainty-aware classification task. As shown in Figure S1, the distribution of T_c values in Supercon is skewed, with a large number of materials having T_c s close to 0 K. We choose to discretize T_c into three categories, based roughly on tertiles: materials with a measured T_c less than 2 K, materials with a T_c between 2 K and 20 K, and materials with a T_c above 20 K.

Our Representation learning from Stoichiometry (RooSt) models (6) incorporate two sources of uncertainty in their T_c predictions: We account for aleatoric uncertainty by letting a model estimate a mean and standard deviation for each label’s logit (7), and we incorporate epistemic uncertainty by averaging over an ensemble of independently trained RooSt models (8).

SuperCon provides data as a validation experiment for our model – can RooSt successfully predict the T_c tertile of unknown materials? We evaluate this question in two settings; the first under a standard uniform cross-validation (Uniform-CV) split of SuperCon, and the second with the leave-one-cluster-out cross validation (leave-one-cluster-out cross-validation (LOCO-CV)) strategy (9). In this approach, we apply K -means clustering to the Magpie (4) representation of SuperCon and then train K RooSt models, iteratively holding out each cluster as a test set. Since the clustering will put materials that are similar to each other in the same cluster, LOCO-CV is a better proxy for assessing how well our model will perform when used to identify superconductor candidates in Materials Project.

In this study, we set $K = 3$ for the clustering and summarize cluster characteristics in Table S2 and Figure S2. Note that even this simple clustering procedure has produced inter-cluster heterogeneity – e.g., Cluster 0 is significantly smaller than the other clusters, and Cluster 1 has the bulk of the $20 \leq T_c$ superconductors.

In Figures S3 and S4, we show the results of our study. In the Uniform-CV setting, our model does well – it shows little evidence of overfitting and performs well for all three T_c categories. However, in LOCO-CV, performance degrades significantly and is also much more variable, based on what cluster is being used as the test set. Our result here echoes (2), who show that models trained only on iron-based superconductors fail to accurately predict properties of cuprates, and vice versa.

These results indicate that we should not expect an ML model trained only on SuperCon to consistently identify superconductors in out-of-distribution data, and, as points in SuperCon are more similar to each other than points in Materials Project (Figure 1 of the main text), the LOCO-CV results here are optimistic compared to our actual problem of interest. This motivates our need for multiple iterations of model training, candidate selection, candidate synthesis, and model retraining.

C. Message-passing over stoichiometry graphs. Here we go into more detail about the approach used in RooSt (6) to map a material composition to a predicted property. The composition is encoded as a fully-connected graph, where each node i corresponds to an atomic species found in that composition. Each species i has an initial representation vector h_i^0 specified by the user (e.g., a one-hot encoding of species type), and the fraction w_i of the composition it makes up (e.g., for $\text{Zr}_3\text{Fe}_4\text{Sn}_4$, $w_{\text{Zr}} = 3/15$). A series of $t = 0, \dots, T - 1$ message-passing updates iteratively update each species representation vector to h_i^{t+1} as follows:

$$\begin{aligned} e_{i,j}^{t,m} &= f^{t,m}(h_i^t, h_j^t) \\ a_{i,j}^{t,m} &= \frac{w_j \exp(e_{i,j}^{t,m})}{\sum_k w_k \exp(e_{i,k}^{t,m})} \\ h_i^{t+1} &= h_i^t + \sum_{m,j} a_{i,j}^{t,m} g^{t,m}(h_i^t, h_j^t), \end{aligned}$$

where i and j are species indices, $f^{t,m}$ and $g^{t,m}$ are multi-layer perceptrons, $a_{i,j}^{t,m}$ are soft attention coefficients computed with a weighted softmax, and the index m denotes separate “attention heads” that stabilize training and improve model expressivity.

The final species representation vectors h_i^T are gathered into a material-level representation vector h after a final soft-attention

operation and then fed through a final MLP f^y to yield a predicted property \hat{y} :

$$\begin{aligned} e_i^{T,m} &= f^{T,m}(h_i^T) \\ a_i^{T,m} &= \frac{w_i \exp(e_i^{T,m})}{\sum_j w_j \exp(e_j^{T,m})} \\ h &= \sum_{m,i} a_i^{T,m} g^{T,m}(h_i^T) \\ \hat{y} &= f^y(h) \end{aligned}$$

Note that pure (unary) elemental materials are not amenable to this representation and cannot be ingested by a RooSt model.

All of the model's weights for the message-passing and prediction mechanisms (i.e., each $f^{t,m}$ and $g^{t,m}$, and f^y , are trained in an end-to-end manner using a cross-entropy loss.

D. Synthesis details. For arc melting, more volatile components were wrapped in metallic foils of less-volatile components and melted with a full-scale current of ~ 50 - 100 A with ~ 0.7 atm argon present in the vacuum chamber. Zirconium metal, which reacts quickly with oxygen, was first melted in the chamber after it was filled with argon to remove any remaining oxygen before the samples were melted. Samples were melted 2-3 times, flipped, and then melted 2-3 times. If evidence of a superconducting transition was observed, homogenizing heat treatments were performed at temperatures that depended on the chemistry of the sample (generally near 1000°C for times ranging from overnight to several days).

For metals containing magnesium or calcium, due to their tendency to vaporize, arc melting was not feasible. CaIn_6Cu_6 , $\text{Ca}(\text{Al}_2\text{Cu})_4$, $\text{Ca}(\text{AgGe})_2$, $\text{Ca}_2\text{Zn}_3\text{Ag}$, $\text{Ca}_3(\text{Cu}_2\text{Sn})_4$, and CaCu_9Sn_4 were made by wrapping samples in tantalum foil (to minimize reactions with the quartz ampoule) and sealing them in evacuated quartz ampoules. The samples were then heated to 700°C for 2 h and the furnace was turned off and allowed to naturally cool. The same was done for $\text{Ca}_3(\text{Cu}_2\text{Sn})_4$, CaCu_9Sn_4 , $\text{Ca}(\text{CuSi}_{0.33}\text{Sn}_{0.33}\text{Ge}_{0.33})_2$, $\text{Ca}_2\text{Zn}_3\text{Ag}$, and $\text{Ca}(\text{AgGe})_2$ except the anneal was performed at 900°C . Vaporization of magnesium in ampoules was more of an issue for the Mg-containing samples compared to calcium vaporization in the Ca-containing samples. Samples with nominal MgCuSn, and MgCuBi compositions were similarly wrapped in tantalum foil and sealed in evacuated quartz ampoules. The samples were then heated in a box furnace to 900°C for 2 h. The furnace was then turned off and the samples allowed to cool to room-temperature. Since tantalum foil has a T_c of 4 K, it was important to separate the samples from the foil before measuring AC susceptibility. This was much more difficult for some of the Mg-containing samples so we also attempted to make MgCuSn and $\text{Mg}_2\text{Cu}_3\text{Si}$ wrapped in molybdenum foil using the same procedures. These samples tended to react with the molybdenum foil and, therefore, did not form the targeted phases.

E. Isolating the new Zr-In-Ni superconductor. The superconducting signal was observed both in single crystals and arc melted samples with indium-rich compositions containing ZrNi_2In , indium, and $\text{Zr}_2\text{Ni}_2\text{In}$, although the strength of this transition varied throughout a given sample and between samples with the same nominal composition. Nominally $\text{Zr}_2\text{Ni}_2\text{In}$ samples confirmed to contain $\text{Zr}_2\text{Ni}_2\text{In}$ did not superconduct at all. The T_c of indium is well-known and cannot explain the ~ 9 K signal. As the strength of the applied static magnetic field was increased to suppress superconductivity in indium, the higher-temperature transition remained and shifted to around 7.1 K. This is what one would expect for a major superconducting phase. Further work is necessary to clarify the precise phase responsible for the superconducting signal. It is clear that, if it is a ZrNi_2In -related phase contributing to the signal, indium-rich stoichiometries are necessary for there to be a significant fraction of the superconducting phase since the signal was weak in relatively phase-pure ZrNi_2In and gained strength under more indium-rich conditions.

Insights into the source of the ~ 9 K transition can be gained by examining the broader Zr-Ni-Al-Ga-In system. A similar 8-9 K phase transition has been observed in mixed $\text{ZrNi}_2\text{Al}_x\text{Ga}_{1-x}$ alloys (10). The T_c 's of ZrNi_2Al and ZrNi_2Ga in that work matched prior reports ($T_c \sim 3$ K for ZrNi_2Ga , $T_c \sim 2$ K for ZrNi_2Al), demonstrating that the elevated T_c is related to Al-Ga alloying. Such behavior was only observed for substitution on the column-13 site (10). A clear increase in the 8-9 K signal was observed when the Al/Ga ratio decreased from 1 to 0.25. This suggests that Heusler alloys are capable of superconducting with onset temperatures near 8-9 K. Furthermore, this observed behavior is not caused by random impurities or air leaks. Due to the sensitivity of the volume fraction of the new Zr-In-Ni superconductor reported here to different processing conditions, it is likely that the responsible phase is highly sensitive to order or disorder and is easy to miss without a thorough analysis.

One alternate explanation of the ~ 9 K signal that we investigated in detail was the possibility of ZrN traces contributing to the signal. Gold-colored flecks were observed in some of the strongly superconducting arc melted samples and cubic ZrN is the only known gold-colored phase that had any chance of being present. Cubic ZrN has a T_c of 9.8-10.0 K, so an air leak might explain the observed ~ 9 K T_c (11). Samples shown by XRD to definitively contain ZrN (Zr_2InNi and ZrNi , melted under nitrogen) showed a T_c below 6 K. No superconducting transition was observed in ZrNi samples melted under argon, demonstrating that indium is necessary for the ~ 9 K T_c .

The strongest signal that we achieved in arc melted samples came from a sample melted under argon and annealed for 5.5 days at 1000°C . This anneal allowed indium to vapor transport away from the bulk of the sample. Parts of the sample with a shiny gray and gold appearance had a comparatively strong superconducting signal (Figure S6a).

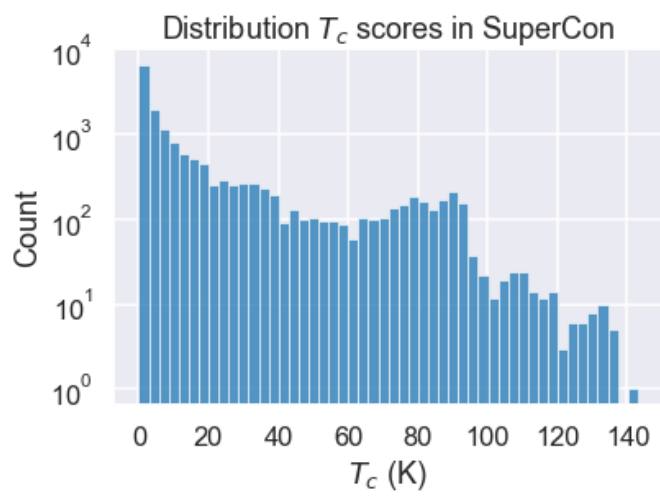


Fig. S1. Distribution of raw T_c values in the version of SuperCon used as training data. The data are long-tailed with a small number of high- T_c outliers.

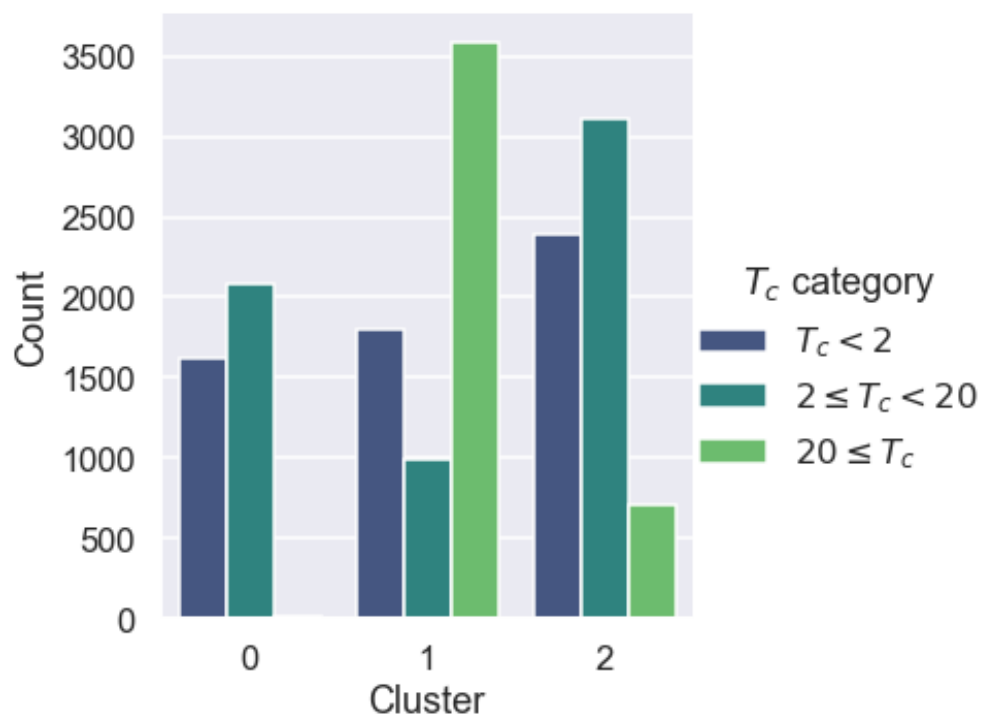


Fig. S2. Statistics of T_c across clusters used in LOCO-CV study

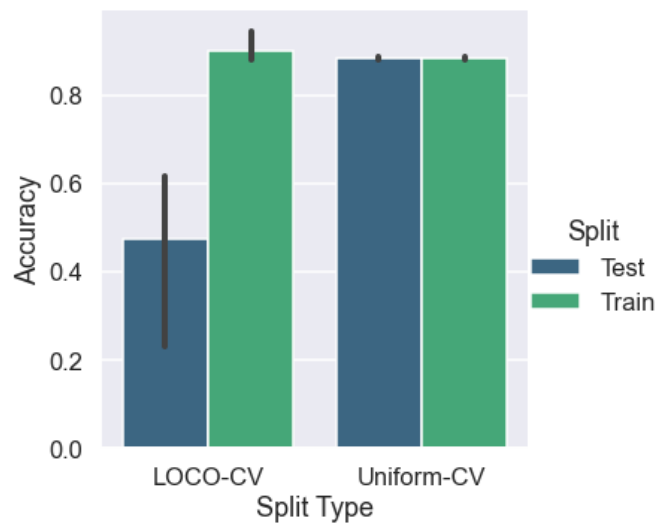


Fig. S3. Training and test set accuracies for Uniform-CV vs. LOCO-CV, averaged over each fold and clusters. Bars show 95% confidence intervals for the standard error of the mean estimate. The model severely overfits in the LOCO-CV case, and its test set accuracy is much more cluster-dependent and variable.

	$T_c < 2$	$2 \leq T_c < 20$	$20 \leq T_c$
# Materials	5,802	6,182	4,320

Table S1. Distribution of T_c values by tertile in our classification formulation. We treat the prediction problem as a three-class classification problem.

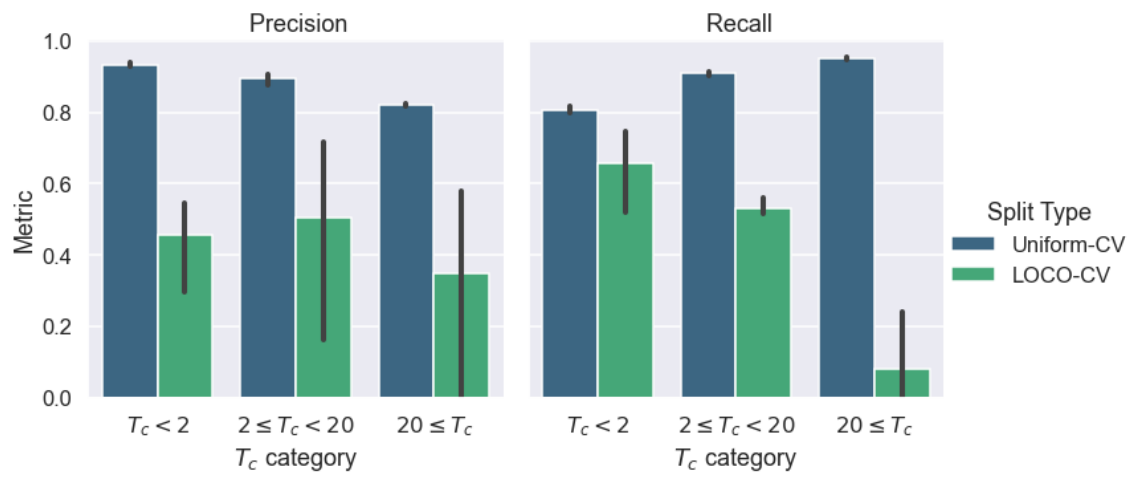


Fig. S4. Test set precision and recall analysis for each T_c category for the uniform vs. LOCO-CV study, averaged over each fold and cluster. Bars show 95% confidence intervals for the standard error of the mean estimate. The model's metrics are much more variable and cluster-dependent for the LOCO-CV model.

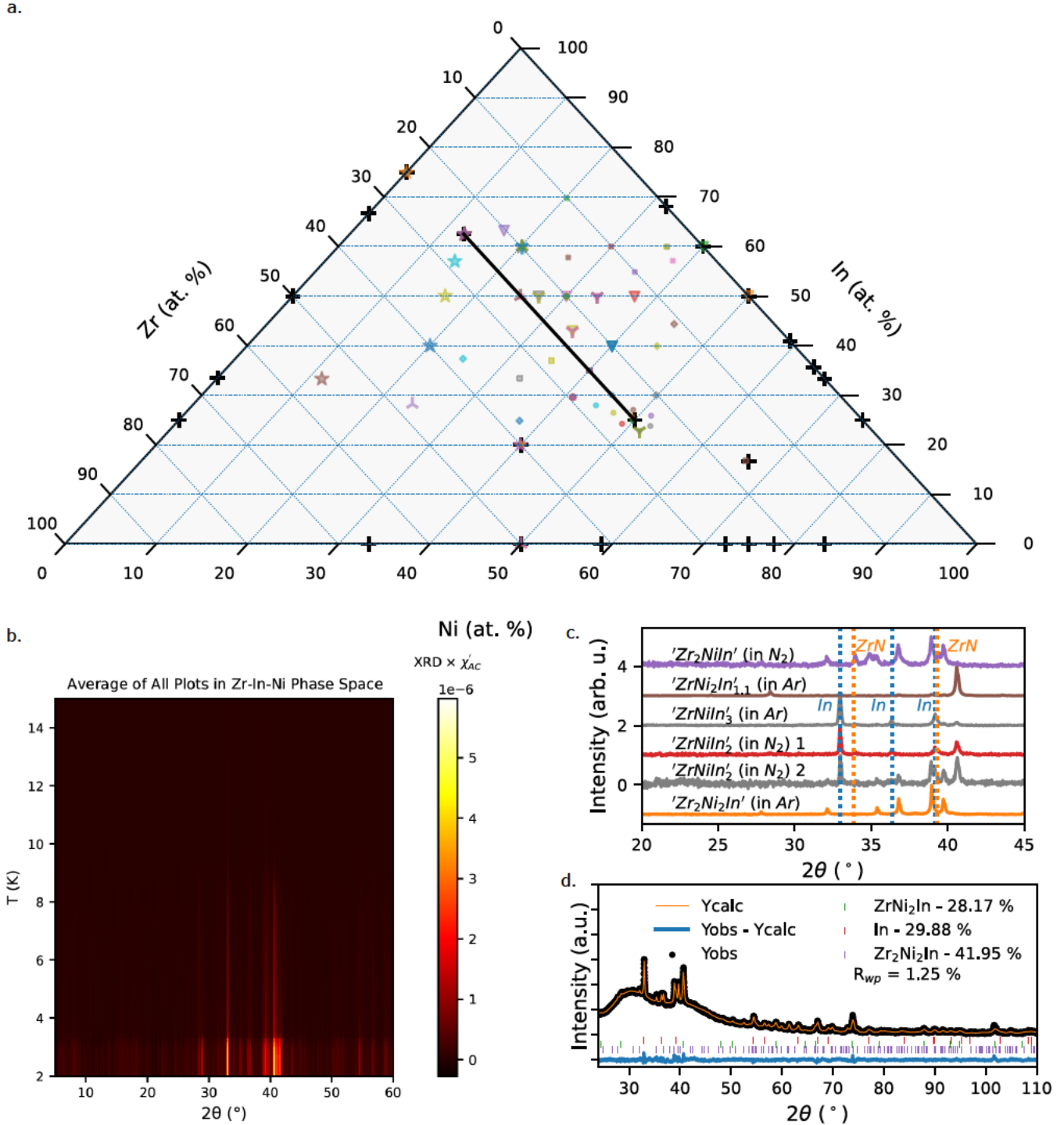


Fig. S5. Samples from around the Zr-In-Ni phase diagram (a) were made, including several binary alloys. XRD data was used with the χ'_{AC} data to identify the new superconductor in the Zr-In-Ni system. (b) shows a heat map averaged over all the samples in the system where the color equals the normalized XRD intensity multiplied by χ'_{AC} ($color = -\chi'_{AC} \times Intensity_{XRD}$). Indium is consistently present in samples with strong superconducting signals below 3.4 K but cannot explain the ~ 9 K transition that is consistently observed. (c) and (d) show how XRD was used to identify the phases present in samples with and without strong superconducting signals. Indium diffraction peaks were used as an internal standard to correct for sample height variations since In-rich samples were extremely malleable and could not be made into a powder. The nominally ZrNi₂In_{1.1} sample contained only indium and ZrNi₂In. The nominally Zr₂Ni₂In sample was primarily Zr₂Ni₂In. Reitveld refinements of samples containing a strong superconducting signal (d) showed indium, ZrNi₂In, and Zr₂Ni₂In present. Our Zr₂Ni₂In sample did not superconduct, implying that ZrNi₂In does superconduct under certain indium-rich conditions. To rule out ZrN impurities as the superconducting phase, a number of samples were melted in nitrogen. Samples intentionally made with the largest amount of ZrN present based on XRD had a T_c below 6 K and, therefore, ZrN impurities would not explain the ~ 9 K transition.

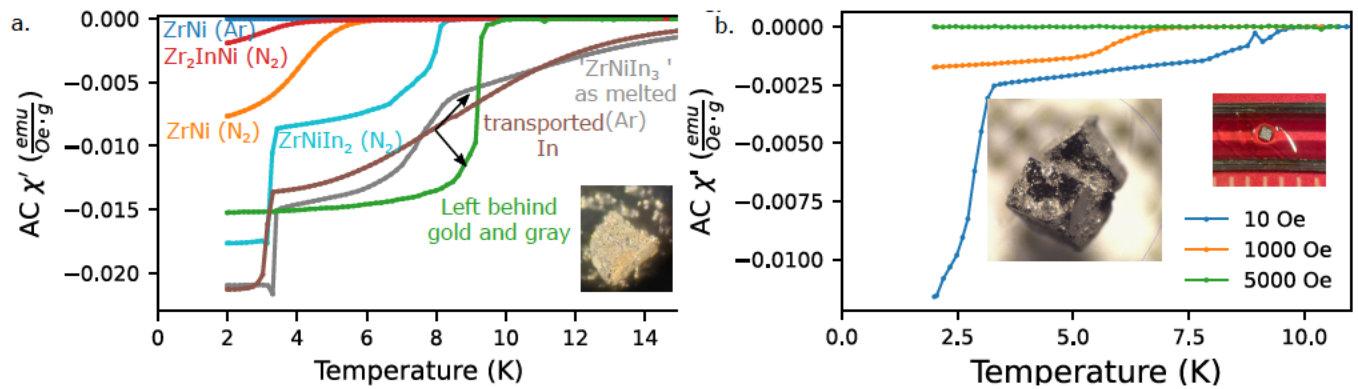


Fig. S6. The existence of the ~ 9 K signal was robust for both arc melted samples and single crystals. To rule out ZrN impurities as the source of the superconducting signal, we arc melted samples of ZrNi and Zr_2NiIn , and ZrNiIn_2 stoichiometry under nitrogen (a). ZrN was identified using XRD in these samples. When ZrNi was melted under argon like most of our samples containing the ~ 9 K signal, no superconducting transition was observed. The ~ 9 K signal was only visible in the sample with a nominal ZrNiIn_2 composition, indicating that indium-rich compositions are required for the ~ 9 K transition to appear. Indium acted as a useful internal standard such that the strength of its superconducting signal could be compared to the strength of the ~ 9 K signal to determine the relative fraction of sample that superconducts at different temperatures. The strength of the indium signal is relatively comparable to the strength of the ~ 9 K signal (when indium could be clearly observed using XRD), indicating that the ~ 9 K transition is a bulk behavior. Furthermore, when indium was vapor transported away from the bulk of an indium-rich sample arc melted under argon, the leftover bulk of material exhibited a strong superconducting signal without indium. A photo of this material is shown in (a). Single crystals grown in an indium flux (b) contained varying amounts of the ~ 9 K superconducting phase, demonstrating that some amount of the ~ 9 K superconductor forms in materials made using vastly different growth techniques. As the magnetic field increased, the ~ 9 K signal shifted to lower temperatures and, by 5000 Oe, disappeared. This is further evidence that the ~ 9 K transition is a bulk behavior.

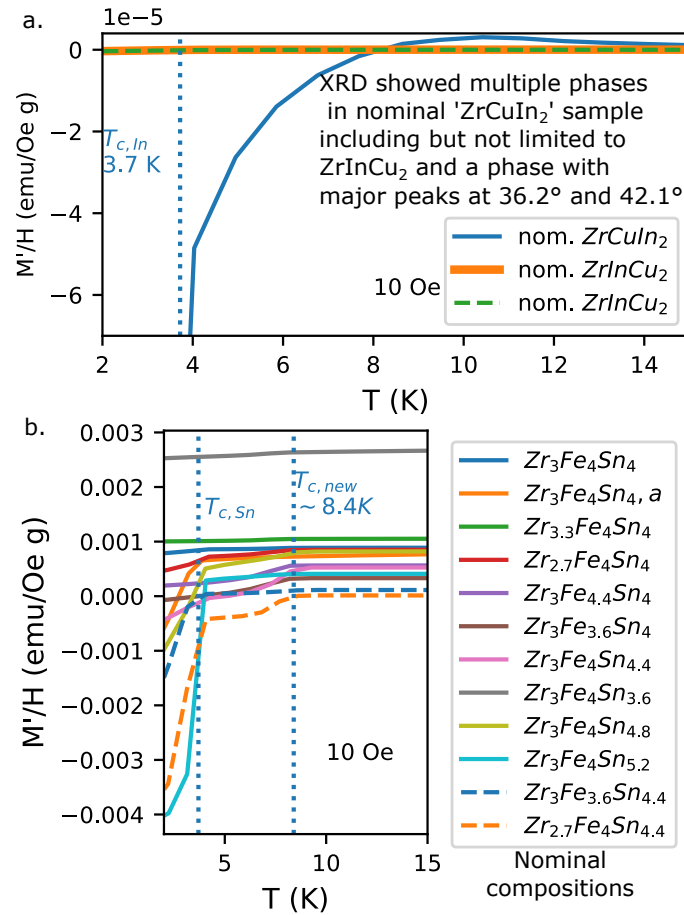


Fig. S7. We saw similar anomalous signals in nominally ZrCuIn₂ and Zr₃Fe₄Sn₄ samples but the superconducting signals also proved difficult to isolate.

Cluster	Size
0	3,723
1	6,377
2	6,204

Table S2. Sizes of clusters used in LOCO-CV study

Table S3. Precursor List

Element or Compound	Source	Form	Purity
Mg	Alfa Aesar	turnings, 3.2 mm wide	99.8%
MgSi ₂	Beantown Chemical	powder	99.5%
Ca	Alfa Aesar	granules, -16 mesh	99.5 %
Sc	Alfa Aesar	pieces	99.9 %
Ti	Alfa Aesar	foil, 0.25 mm	99.5 %
Zr	Strem	foil	99.8%
Hf	Alfa Aesar	foil, 0.025 mm	99.5 %
V	Alfa Aesar	foil, 0.127 mm	99.8 %
	Alfa Aesar	wire, 1.5 mm	99.8 %
Nb	Alfa Aesar	foil, 0.3 mm	99.8 %
	Alfa Aesar	foil, 0.025 mm	99.8 %
	Strem	foil	99.8 %
Ta	Alfa Aesar	foil, 0.025 mm	99.95 %
	Beantown Chemical	foil, 0.025 mm	99.95 %
Mo	Beantown Chemical	foil, 0.025 mm	99.95 %
W	Alfa Aesar	wire, 0.75 mm diameter	99.95 %
Mn	Beantown Chemical	pieces	99.95 %
Fe	Goodfellow	foil	99.8 %
Co	Alfa Aesar	pieces	99.9+ %
Co	Aldrich	pieces	99.5 %
Ni	Alfa Aesar	foil	99+%
	Alfa Aesar	-300 mesh	99.8%
Cu	Strem	foil	99.9 %
	Alfa Aesar	powder, -325 mesh	99%
	Alfa Aesar	shot, 4-6 mm, Pufratronic	99.999%
Ag	Alfa Aesar	wire	99.9 %
Zn	Alfa Aesar	ingot	99.99 %
B	Alfa Aesar	powder, -325 mesh	98 %
Al	Beantown Chemical	wire, 1.0 mm diameter	99.999 %
Ga	NOAH Tech	chunks	99.99 %
In	Alfa Aesar	shot, 4 mm tear drop	99.99 %
C	Alfa Aesar	graphite rod, 6.15 mm diameter	99.9995%
Si	Alfa Aesar	lump	99.999+%
Ge	Beantown Chemical	pieces, 3-9 mm	99.999%
Sn	Beantown Chemical	shot (8-20 mesh)	99.5 %
	Beantown Chemical	granules	99.9 %
Pb	Alfa Aesar	pieces	99.999 %
P	Sigma Aldrich	red, powder	97+%
Bi	Alfa Aesar	needles, 1-5 cm, 1.5 mm diameter	99.99%
S	Alfa Aesar	powder, Puratronic	99.999%
Yb	Alfa Aesar	pieces, sublimed	99.9 %

References

1. Roter, B., Dordevic, S.V.: Predicting new superconductors and their critical temperatures using machine learning. *Physica C: Superconductivity and its Applications* **575**, 1353689 (2020). <https://doi.org/10.1016/j.physc.2020.1353689>. Accessed 2021-10-11
2. Stanev, V., Oses, C., Kusne, A.G., Rodriguez, E., Paglione, J., Curtarolo, S., Takeuchi, I.: Machine learning modeling of superconducting critical temperature. *npj Computational Materials* 2018 4:1 **4**, 1–14 (2018). <https://doi.org/10.1038/s41524-018-0085-8>
3. Konno, T., Kurokawa, H., Nabeshima, F., Sakishita, Y., Ogawa, R., Hosako, I., Maeda, A.: Deep Learning Model for Finding New Superconductors. *Phys. Rev. B* **103**(1), 014509 (2021). <https://doi.org/10.1103/PhysRevB.103.014509>. arXiv: 1812.01995. Accessed 2021-10-11
4. Ward, L., Agrawal, A., Choudhary, A., Wolverton, C.: A general-purpose machine learning framework for predicting properties of inorganic materials. *npj Computational Materials* **2**(1), 16028 (2016). <https://doi.org/10.1038/npjcompumats.2016.28>
5. Jha, D., Ward, L., Paul, A., Liao, W.-k., Choudhary, A., Wolverton, C., Agrawal, A.: Elemnet: Deep learning the chemistry of materials from only elemental composition. *Scientific Reports* **8**(1), 17593 (2018). <https://doi.org/10.1038/s41598-018-35934-y>
6. Goodall, R.E.A., Lee, A.A.: Predicting materials properties without crystal structure: deep representation learning from stoichiometry. *Nature Communications* 2020 11:1 **11**, 1–9 (2020). <https://doi.org/10.1038/s41467-020-19964-7>
7. Nix, D.A., Weigend, A.S.: Estimating the mean and variance of the target probability distribution. In: *Proceedings of 1994 IEEE International Conference on Neural Networks (ICNN'94)*, vol. 1, pp. 55–601 (1994). <https://doi.org/10.1109/ICNN.1994.374138>
8. Lakshminarayanan, B., Pritzel, A., Blundell, C.: Simple and scalable predictive uncertainty estimation using deep ensembles. In: *Proceedings of the 31st International Conference on Neural Information Processing Systems. NIPS'17*, pp. 6405–6416. Curran Associates Inc., Red Hook, NY, USA (2017)
9. Meredig, B., Antono, E., Church, C., Hutchinson, M., Ling, J., Paradiso, S., Blaiszik, B., Foster, I., Gibbons, B., Hattrick-Simpers, J., Mehta, A., Ward, L.: Can machine learning identify the next high-temperature superconductor? examining extrapolation performance for materials discovery. *Mol. Syst. Des. Eng.* **3**, 819–825 (2018). <https://doi.org/10.1039/C8ME00012C>
10. Basaula, D.R.: Superconducting Properties of $ZrNi_{2-x}TM_xGa$ and $ZrNi_2Al_xGa_{1-x}$ Heusler Compounds. Masters, Miami University (2018)
11. Lengauer, W.: Characterization of nitrogen distribution profiles in fcc transition metal nitrides by means of Tc measurements. *Surface and Interface Analysis* **15**(6), 377–382 (1990). <https://doi.org/10.1002/sia.740150606>